Engineering of spatial solitons in two-period QPM structures

Steffen Kjær Johansen*, Silvia Carrasco, and Lluis Torner

Laboratory of Photonics, Department of Signal Theory and Communications, Universitat Politecnica de Catalunya, Gran Capitan UPC-D3, Barcelona, ES 08034, Spain

Ole Bang

Department of Informatics and Mathematical Modelling, Technical University of Denmark, DK-2800 Lyngby, Denmark

Abstract

We report on a scheme which might make it *practically* possible to engineer the effective competing nonlinearities that on average govern the light propagation in quasi-phase-matching (QPM) gratings. Modulation of the QPM period with a second longer period, introduces an extra degree of freedom, which can be used to engineer the effective quadratic and induced cubic nonlinearity. However, in contrast to former work here we use a *simple phase-reversal grating* for the modulation, which is practically realizable and has already been fabricated. Furthermore, we develop the theory for *arbitrary relative lengths of the two periods* and we consider the effect on solitons and the bandwidth for their generation. We derive an expression for the bandwidth of multicolor soliton generation in two-period QPM samples and we predict and confirm numerically that the bandwidth is broader in the two-period QPM sample than in homogeneous structures.

Quasi-phase-matching (QPM) is a major alternative over conventional phase matching in many laser applications based on frequency-conversion processes in quadratic nonlinear media (for reviews, see (1; 2)). Besides other practical advantages, QPM allows tailoring the nonlinearity of the material to form complex structures. This opens a range of new possibilities, which have become experimentally feasible with the recent progress in poling techniques. For example, engineerable pulse compression in frequency-doubling schemes in synthetic QPM gratings has been demonstrated in aperiodically poled lithium niobate and potassium niobate (3; 4; 5; 6), and transverse QPM gratings have been made both for shaping second-harmonic beams and to extend the spectral coverage of optical parametric oscillators(7; 8). Bandwidth enhanced parametric

interactions can be obtained in modulated-period structures (9), multiple nonlinear interactions can be achieved in quasi-periodic schemes (10; 11; 12; 13), and simultaneous generation of multiple color laser light has been demonstrated in QPM crystals doped with active lasing ions (14). QPM engineering also finds novel important applications beyond pure frequency-conversion devices, e.g., to generate enhanced cascading phase-shifts (15), all-optical diode operation (16), and multicolor soliton formation (17; 18; 19; 20; 21; 22).

Here we show that two-period QPM structures offer new opportunities for soliton control.

Multicolor solitons mediated by second-harmonic generation (SHG) form by mutual trapping of the beams at the fundamental frequency (FF) and at the second harmonic frequency (SH). Here we focus on bright solitons whose basic properties are well known. Whole dynamically stable families exist above a certain power threshold for all phase mismatches. At lowest order the effect of QPM grating is to average the quadratic nonlinearity (2). However, taking higher order perturbations into account reveals that the corresponding averaged field equations include effective cubic, Kerr-like terms(19; 23; 24). Such terms modify the average properties of CW waves (25; 26) and the soliton families of the averaged equations (19; 24; 27), which can be analyzed as sustained by competing quadratic and effective cubic nonlinearities (28; 29; 30; 31; 32).

Nevertheless, in standard QPM the strength of the induced averaged cubic nonlinearity is proportional to the ratio between the QPM grating period and the soliton characteristic length (i.e., the diffraction length in the case of spatial solitons). At optical wave lengths, the former is typically of the order of ten μm, whereas the latter is a few mm. Therefore, the strength of the induced cubic nonlinearities is extremely small. The question thus naturally arises whether and how QPM engineering can be employed to bring the effective cubic nonlinearities to compete with the quadratic in the average fields. One solution is to add a strong dc-part to the nonlinear QPM grating, i.e. as done in (33; 34). This adds a term to the induced Kerr terms, which is proportional to the QPM grating period and the dc-value squared, and thus can be large(24). Another potentially more versatile technique is to modulate the QPM period with a second longer period, as it was shown theoretically in (23). This introduces an extra degree of freedom, which can be used to engineer the effective quadratic and induced averaged cubic nonlinearity.

Here we consider the latter technique. However, in contrast to the rather complicated long-period modulation used in (23) we use here a *simple phase-reversal grating* for the modulation, similar to the two-period QPM sample recently employed by Chou and co-workers (12) for multiple-channel wavelength conversion in the third telecommunication window. Furthermore, we develop the theory for *arbitrary relative lengths of the two periods* and we consider the effect of the modulation on multicolor solitons. We expect soliton formation to be possible for a variety of phase-reversal periods, in view of the fact that multicolor solitons have been shown to be robust against strong perturbations, including quasi-periodic QPM gratings(21) and even periodic gain

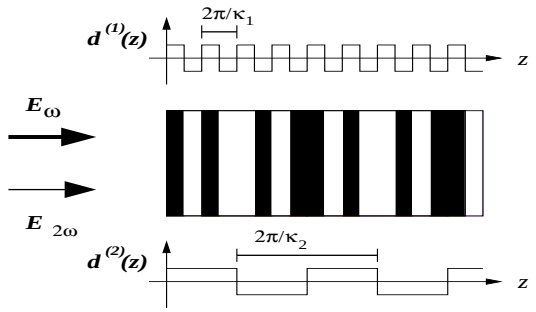

Fig. 1. Two-period QPM grating.

and loss(35). Using the induced averaged cubic nonlinearities we derive an expression for the bandwidth of multicolor soliton generation in two-period QPM samples and we show that the bandwidth is broader in the two-period QPM sample than in homogeneous quadratic nonlinear materials. Importantly, all our results are confirmed numerically.

We consider beam propagation under type-I SHG conditions in a lossless QPM $\chi^{(2)}$ slab waveguide. The slowly varying envelope of the fundamental wave, $E_1 = E_1(x, z)$, and its SH, $E_2 = E_2(x, z)$, are(36)

$$i\frac{\partial E_1}{\partial z} + \frac{1}{2}\frac{\partial^2 E_1}{\partial x^2} + d(z)E_1^* E_2 e^{-i\beta z} = 0, \tag{1}$$

$$i\frac{\partial E_2}{\partial z} + \frac{\alpha}{2}\frac{\partial^2 E_2}{\partial x^2} + d(z)E_1^2 e^{i\beta z} = 0, \tag{2}$$

where in all cases of practical interest $\alpha \simeq 0.5$. The normalized wave-vector mismatch is introduced via the real parameter $\beta = k_1\omega_0^2\Delta k$, where $\Delta k = 2k_1 - k_2$, and ω_0 is the beam width, and $k_{1,2}$ are the linear wave numbers of the fundamental and SH, respectively. The scaled transverse coordinate, x, is measured in units of ω_0 and the propagation coordinate, z, is measured in units of $2l_d$ where $l_d = k_1\omega_0^2/2$ is the diffraction length of the fundamental wave. The spatial periodic modulation of the nonlinearity is described by the grating function $d(z)$ whose amplitude is normalized to 1, and whose domain length we define as $\Lambda = \pi/\kappa$, where κ is the spatial grating frequency or the QPM frequency, which we assume real and positive. In the case of second-harmonic generation in lithium niobate pumped at $\lambda_\omega \sim 1.5$ μm with a beam width of $\omega_0 \sim 20$ μm, the intrinsic material wave vector mismatch is of the order $|\beta| \sim 10^3$. Thus the QPM frequency must also be of this order which corresponds to a domain length of ~ 10 μm. For such values, a scaled grating frequency of the order $\kappa \sim 10$ correspond to a domain length of about 1 mm.

The two-period grating function, $d(z)$, consists of a primary grating, $d^{(1)}(z)$, and a superimposed secondary grating, $d^{(2)}(z)$. We expand $d(z)$ in a Fourier series

$$d(z) = \sum_k d_k^{(1)} \exp(ik\kappa_1 z) \times \sum_l d_l^{(2)} \exp(il\kappa_2 z) \tag{3}$$

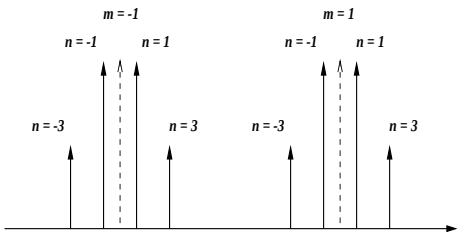

Fig. 2. Peak splitting in the two-period QPM grating. Dashed peaks indicate the location of the 1'st order peaks in the one-period case.

where the summations are over all (k, l) from $-\infty$ to ∞. If we assume the grating functions to be square, only the odd harmonics enters into the expansion, $d_{2l+1} = 2/i\pi(2l+1)$ and $d_{2l} = 0$. In the case of low-depletion SHG, the effect of the superimposed period is to split each peak of the original one-period QPM grating into an infinite family of peaks(12). More formally, one has peaks at all spatial QPM frequencies $m\kappa_1 + n\kappa_2$ where m and n are the QPM orders related to the primary and secondary grating, respectively. These peaks are not delta-like, though for simplicity they are depicted as such in Fig. 2, but rather sinc-like functions around the relevant QPM frequency. The SHG-efficiency is higher the lower the order. Hence, in one-period QPM one would choose to match to the first peak ($m = \pm 1$). In two-period QPM there is an equivalent rule, i.e. the low-depletion SHG-efficiency is highest for $m = n = \pm 1$. To be able to treat the problem mathematically we have to neglect all overlap between peaks in order to avoid resonances. Thus we must assume $\kappa >> 1$ in the one-period case. In the general two-period case the spectrum becomes dense, as in the case of a Fibonacci grating(21). In order to be able to neglect any overlap between the peak we are looking at, and the rest of the dense spectrum, we have to assume, not only high spatial QPM frequencies, but also that the two frequencies are of different order. We remark that soliton excitation is expected to be possible no matter what the spectrum looks like, as long as the power is high enough(21). Our numerical simulations presented here agree with this expectation. It is the lack of analytical tools which necessitates the assumption of well separated peaks.

By applying the asymptotic expansion(37) technique we have established a perturbation theory describing the propagation of the averaged fields in this two-period QPM system. We make the transformation $E_1(x, z) = w(x, z)$ and $E_2(x, z) = v(x, z) \exp(i\epsilon z)$, where $\epsilon = \beta - m\kappa_1 - n\kappa_2$, is the residual phase mismatch, which is assumed to be small. The functions $w(x, z)$ and $v(x, z)$ are assumed to vary slowly on the scale given by the QPM periods and can be expanded in the Fourier series

$$w(x,z) = w_0(x,z) + \sum_{k\neq 0} w_k(x,z)e^{ik\kappa_1 z} + \sum_{l\neq 0} \omega_l(x,z)e^{il\kappa_2 z}, \tag{4}$$

$$v(x,z) = v_0(x,z) + \sum_{k\neq 0} v_k(x,z)e^{ik\kappa_1 z} + \sum_{l\neq 0} \nu_l(x,z)e^{il\kappa_2 z}. \tag{5}$$

We remark that this assumption is valid also when the QPM frequencies share

common harmonics. In this case the SHG spectrum discussed above becomes discrete as in the one-period case. However, to avoid overlap between peaks the QPM frequencies must still be assumed of different order. Furthermore we formally assume that $\beta >> 1$, $\kappa_1 >> 1$, and $\kappa_2 >> 1$. Substituting (4-5) into (1-2) and matching leading order terms yields the relations for the harmonic coefficients(19). One gets

$$w_q = \frac{1}{q\kappa_1} d_n^{(2)} d_{(q+m)}^{(1)} w_0^* v_0, \quad v_n = \frac{1}{q\kappa_1} d_{-n}^{(2)} d_{(q-m)}^{(1)} w_0^2, \tag{6}$$

$$\omega_q = \frac{1}{q\kappa_2} d_m^{(1)} d_{(q+n)}^{(2)} w_0^* v_0, \quad \nu_n = \frac{1}{q\kappa_2} d_{-m}^{(1)} d_{(q-n)}^{(2)} w_0^2, \tag{7}$$

and the equations governing the averaged fields are of the form

$$i\frac{\partial w_0}{\partial z} + \frac{1}{2}\frac{\partial^2 w_0}{\partial x^2} + \eta w_0^* v_0 + \gamma(|w_0|^2 - |v_0|^2) w_0 = 0, \tag{8}$$

$$i\frac{\partial v_0}{\partial z} + \frac{1}{4}\frac{\partial^2 v_0}{\partial x^2} - \epsilon v_0 + \eta w_0^2 - 2\gamma |w_0|^2 v_0 = 0. \tag{9}$$

System (8-9) conserves the same power as system (1-2), $P = \int (|w_0|^2 + |v_0|^2) dx = \int (|E_1|^2 + |E_2|^2) dx$. The strengths of the averaged nonlinearities are given by

$$\eta = d_m^{(1)} d_n^{(2)} - \sum_k d_k^{(1)} d_{[(k-m)\frac{\kappa_1}{\kappa_2}+n]}^{(2)}, \tag{10}$$

$$\gamma = \frac{d_{-n}^{(2)}}{\kappa_1} \sum_{q,l} \frac{d_l^{(2)} d_{[(m+q)-(l-n)\frac{\kappa_2}{\kappa_1}]}^{(1)} d_{[m+q]}^{(1)}}{q} + \frac{d_{-m}^{(1)}}{\kappa_2} \sum_{q,k} \frac{d_k^{(1)} d_{[(n+q)-(k-m)\frac{\kappa_1}{\kappa_2}]}^{(2)} d_{[n+q]}^{(2)}}{q}. \tag{11}$$

In these expressions, q, l, and k are integers, and the summations are everywhere over all integers from $-\infty$ to ∞ except zero. We emphasize that the averaged model (8-9) is valid for arbitrary values of κ_1 and κ_2 as long as the assumptions $\kappa_1 >> 1$, and $\kappa_2 >> 1$ are not violated. However care must be taken when calculating the sums in (10) and (11). When necessary, k and l, themselves integers, must always be chosen such that the $(k-m)\kappa_1/\kappa_2$ and $(l-n)\kappa_2/\kappa_1$ are integers. This ensures that the Fourier coefficients $d_k^{(1)}$ and $d_l^{(1)}$ exist. We remark that if one of the QPM frequencies is an irrational number expressions (10) and (11) are greatly simplified

$$\eta = d_m^{(1)} d_n^{(2)}, \tag{12}$$

$$\gamma = \frac{d_n^{(2)} d_{-n}^{(2)}}{\kappa_1} \sum_q \frac{d_{[m+q]}^{(1)^2}}{q} + \frac{d_m^{(1)} d_{-m}^{(1)}}{\kappa_2} \sum_q \frac{d_{[n+q]}^{(2)^2}}{q}. \tag{13}$$

To make the cubic self- and cross-phase modulation symmetric in (8-9) we have had to assume that $d_n^{*(i)} = d_{-n}^{(i)} = -d_n^{(i)}$, which is the case for square grating functions. Otherwise expressions (10-13) hold for any grating function of the form (3). Rewriting (10) and (11) for square grating functions we get

$$\eta = -\frac{4}{\pi^2}\left(\frac{1}{mn} - \sum_s \frac{1}{(2s+m)\left(2s\frac{\kappa_1}{\kappa_2}+n\right)}\right), \tag{14}$$

$$\gamma = -\frac{16}{\pi^4}\left(\frac{1}{n\kappa_1}\sum_{q,r}\frac{1}{2q(2r+n)\left(2q-2r\frac{\kappa_2}{\kappa_1}+m\right)(m+2q)}\right.$$
$$\left. +\frac{1}{m\kappa_2}\sum_{q,s}\frac{1}{2q(2s+m)\left(2q-2s\frac{\kappa_1}{\kappa_2}+n\right)(n+2q)}\right), \tag{15}$$

where the summations now are over all integers q, r, and s from $-\infty$ to ∞ except zero. Notice the different sign of the lowest-order contribution to (14) at the $(m = 1, n = 1)$-peak, and the $(m = 1, n = -1)$-peak. Such change of sign has implications to the soliton features, as shall be discussed below. Equations (8-9) were first derived in (19). They have the same form regardless of the specific type of grating, the parameters still merely being given as sums over the Fourier coefficients of the grating. Thus they were derived in (24) for QPM with both a linear and a nonlinear grating with or without a dc-value of the nonlinear grating. They were also derived in (23) for a more exotic two-period grating.

By letting $w_0(x, z) = \bar{w}(x, z)/\eta$ and $v_0(x, z) = \bar{v}(x, z)/\eta$ we can reduce system (8-9) to

$$i\frac{\partial \bar{w}}{\partial z} + \frac{1}{2}\frac{\partial^2 \bar{w}}{\partial x^2} + \bar{w}^*\bar{v} + \tilde{\gamma}(|\bar{w}|^2 - |\bar{v}|^2)\bar{w} = 0, \tag{16}$$

$$i\frac{\partial \bar{v}}{\partial z} + \frac{1}{4}\frac{\partial^2 \bar{v}}{\partial x^2} - \epsilon\bar{v} + \bar{w}^2 - 2\tilde{\gamma}|\bar{w}|^2\bar{v} = 0. \tag{17}$$

The stationary bright solitary families of system (16-17) are of the form $\bar{w}(x, z) = u_1(x)\exp(i\lambda z)$, $\bar{v}(x, z) = u_2(x)\exp(i2\lambda z)$. They are parametrized by the soliton parameter $\lambda > \max\{0, -\epsilon/2\}$. The stationary solutions of (8-9) are parametrized by exactly the same parameter but since this system is characterized by three (ϵ, η, and γ) rather than the two parameters of (16-17) (ϵ and $\tilde{\gamma} = \gamma/\eta^2$) each solution of (16-17) corresponds to an infinite family of solutions of (8-9), i.e. an infinite number of QPM frequency combinations and thus physical setups. System (16-17) conserves the renormalized power $\bar{P} = \int(|\bar{w}|^2 + |\bar{v}|^2)dx = \eta^2 P$. We note that also the assumed slow variation of the functions $w(x, z)$ and $v(x, z)$ imposes constraints on the choice of the soliton parameter λ. The characteristic soliton scale length, $2\pi/\lambda$, must be much larger than the QPM period $\Lambda = \pi/\kappa$, where κ in the two-period case is the smallest QPM frequency.

Merely looking at expressions (14-15) suggests that in principle there is ample room for engineering of the averaged nonlinearities. The main parameters are the QPM frequencies κ_1 and κ_2. In general we can state that the higher the QPM frequencies are, the lower the induced averaged cubic terms become. Thus $\gamma \to 0$ for $\kappa_1, \kappa_2 \to \infty$. One also notices that the ratio between κ_1 and κ_2 and vice versa plays an important role in the sums in expressions (14) and (15). We observe that the smaller the ratio the more significant

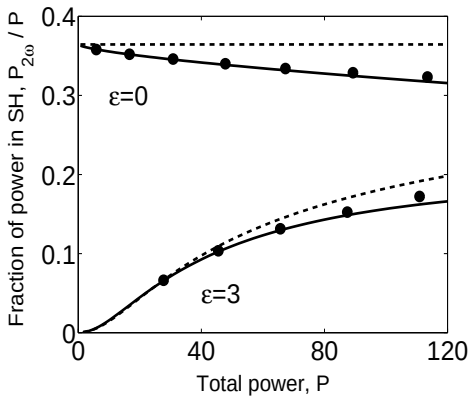

Fig. 3. Fraction of power in the SH for the two-period QPM system with $(\kappa_1, \kappa_2) = (997, 13)$ as a function of total power. Solid line and •: Theoretical and numerically measured values, respectively. Dashed curves: Zero-order approximation, $\gamma = 0$. The value of ϵ is indicated at each pair of curves.

the corresponding sums. From (14) it is obvious that the induced part of the averaged quadratic nonlinearity depends *only* on the ratio κ_2/κ_1. Thus we can realize the same averaged quadratic nonlinearity at large QPM frequencies (no induced averaged cubic terms) and at low QPM frequencies (significant induced averaged cubic terms). We note that if we let the second grating function $d^{(2)}(z) = 1$, the only Fourier coefficient left in the expansion of $d^{(2)}(z)$ is $d_0^{(2)} = d_n^{(2)} = d_{-n}^{(2)} = 1$ and hence $\eta = d_m^{(1)}$ and $\gamma = \frac{1}{\kappa_1} \sum d_{[m+q]}^{(1)^2}/q$. The whole system thus degenerates into the one-period case and the results of (19) are reproduced.

Depending on our objectives we can make the individual terms of the averaged nonlinearities more or less significant. Thus we can essentially make the two-period QPM system behave like the one-period system with induced averaged cubic nonlinearities by choosing $\kappa_1 >> \kappa_2$ while still assuming $\kappa_2 >> 1$. In this way one can use κ_1 to reduce a large intrinsic phase mismatch, β, to a small effective mismatch which can then be manipulated further with κ_2. Thus, if we let $\kappa_1 \to \infty$ the averaged nonlinearities of for the system with square grating functions (14-15) with $m = n = 1$ reduces to

$$\eta = -\frac{4}{\pi^2}, \qquad \gamma = \frac{4}{\kappa_2 \pi^2}\left(1 - \frac{8}{\pi^2}\right) \tag{18}$$

To verify the model in this $\kappa_1 \to \infty$ limit we have made a series of simulations launching soliton initial conditions, found from (16-17), in a real two-period structure described by (1-2) with κ_1 chosen to be a high prime and κ_2 a small prime. Choosing primes effectively eliminates contributions from the remaining sums in (14-15) because r and s must be chosen such that $r\kappa_2/\kappa_1$ and $s\kappa_1/\kappa_2$ are positive integers. We measure the fraction of power in the SH after any initial transient has died out and compare this to the theoretically predicted value. In Fig. 3 we have summarized the results of this investigation for different powers and different effective phase mismatches.

If both QPM frequencies are of the same order, the full non-simplified expres-

sions (14-15) must be used to calculate the averaged nonlinearities. Because of the way the ratio κ_1/κ_2 enters in (14-15), one has *discrete resonances* between the QPM frequencies. At these discrete resonances the induced averaged nonlinearities become stronger. The strength depends on the order of the resonance, the lower the order the higher the strength. To show how the strength of the averaged nonlinearities are calculated we concentrate on the summations involving $s\kappa_1/\kappa_2$. The contribution of the terms involving $r\kappa_2/\kappa_1$ is handled in an analogous way. First-order resonances arise when κ_1/κ_2 is a positive integer; then s is summed over all integers except zero from $-\infty$ to ∞. Second-order resonances arise when $\kappa_1 = (2p-1)\kappa_2/2$ where p is a positive integer. In this case s only spans the even integers. Third-order resonances occur when $\kappa_1 = p * \kappa_2/3$ where $p = 1, 2, 4, 5, 7, 8, \cdots$; then s must be summed over the integers $\pm 3, \pm 6, \pm 9, \cdots$. And so on and so forth for higher-order resonances.

We emphasize that resonances in principle must be taken into account whenever the gratings periods are rational values. In actual practice, the values of the grating periods are not integers but may be approximated by rational numbers. For example, let $(\kappa_1, \kappa_2) = (194.7, 13.3)$. In this particular case, we can write $\kappa_1 = p\kappa_2/133$, where p is any integer which has no common divisor with 133 except 1, showing that we are thus dealing with a 133'rd order resonance. In this particular case, $p = 1947$, and s must be summed over $\pm 133, \pm 266, \pm 399, \cdots$.

In Fig. 4 we show the induced averaged cubic nonlinearity of the reduced system, $\tilde{\gamma} = \gamma/\eta^2$, as a function of the QPM frequency κ_1 (κ_2 is fixed). We have plotted the values for the lowest order resonances together with the no-resonance curve, i.e. the limiting curve where the average nonlinearities are given by (12-13) which in the case of square grating functions reduces to

$$\eta = -\frac{4}{\pi^2}, \tag{19}$$

$$\gamma = \frac{4}{\pi^2}\left(1 - \frac{8}{\pi^2}\right)\left(\frac{1}{\kappa_1} + \frac{1}{\kappa_2}\right). \tag{20}$$

It is evident from Fig. 4 that the higher order resonances quickly converge towards the no-resonance curve with κ_1 and that only the first order resonances yield induced averaged cubic nonlinearity significantly higher than the no-resonance case. We note that the resonance peaks shown are truly discrete. Furthermore, when the grating periods are non-integer numbers, only very high-order resonances occur. The point labelled $\circ$ in Fig. 4 illustrates the idea. It corresponds to $(\kappa_1, \kappa_2) = (8.66, 13)$. While the very similar structure corresponding to $(\kappa_1, \kappa_2) = (26/3, 13)$ yields a third-order resonance contribution, $(\kappa_1, \kappa_2) = (8.66, 13)$ yields a 650th order resonance. Hence, the negligible deviation relative to the no-resonance curve. The conclusion is thus that only the no-resonance curve is of practical experimental interest.

However, to verify that the model is correct we still need to analyze the full resonant structure of the averaged nonlinearities. Thus in Fig. 5 we focus

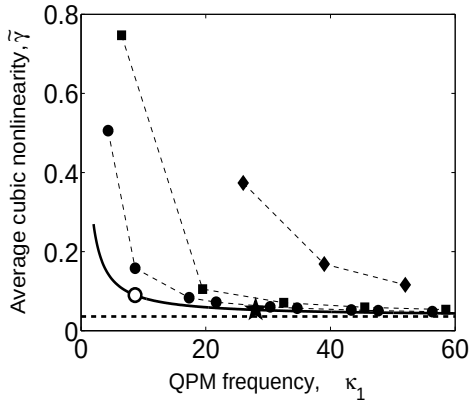

Fig. 4. Averaged cubic nonlinearity at the $(m = n = 1)$-peak in the reduced system as a function of the QPM frequency κ_1 ($\kappa_2 = 13$). Full curve: No-resonance limit. ♦: 1'st order resonances. ■: 2'nd order resonances. •: 3'rd order resonances. The lines between •, ♦ and ■'s are only to help the eye. Dashed line: $\kappa_2 \to \infty$ approximation. ○: Indicates a point, $(\kappa_1, \tilde{\gamma}) = (8.66, 0.090)$ very close to the $p = 2$ 3'rd order resonance point $(\kappa_1, \tilde{\gamma}) = (26/3, 0.157)$. ★: Indicates the point where $\tilde{\gamma} \approx 0.050$ (see text).

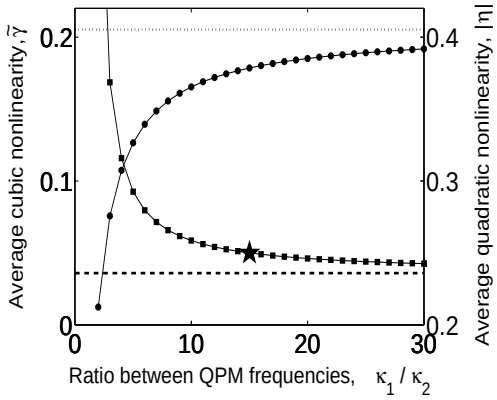

Fig. 5. Averaged nonlinearities at the first order resonances from Fig. 4. $\kappa_2 = 13$ and $\kappa_1 = p * 13$ (p is an integer). ■: The effective cubic nonlinearity, $\tilde{\gamma}$, of the averaged system. •: Amplitude of the averaged quadratic nonlinearity, η. The curves are discrete and the lines in between the •'s and ■'s are just to help the eye. The dashed and dotted lines indicate the asymptotic values of $\tilde{\gamma}$ ($\kappa_1 \to \infty$) and $|\eta|$, respectively. ★ indicates the point where $\tilde{\gamma} \approx 0.050$ (see text).

on the first order resonances and show how the effective averaged quadratic nonlinearity changes with the ratio κ_1/κ_2. In the same figure we have also plotted $\tilde{\gamma}$ to emphasize the interplay between $\tilde{\gamma}$ and η. Recall that the graphs are not continuous but discrete functions of κ_1/κ_2, i.e. the plot only holds for values of κ_1 which are integers of κ_2 ($\kappa_2 = 13$ in this case). In Fig. 6 we have made a series of numerical experiments to confirm that the averaged model derived in this paper does predict correct behavior also at the QPM frequency resonances. Again we launch soliton found from (16-17) in the real system described by (1-2), but now we keep the input power fixed, while we change κ_1 in integer steps of κ_2. Simulations where carried out in the actual two-period QPM structure. As before we let the evolution continue until any

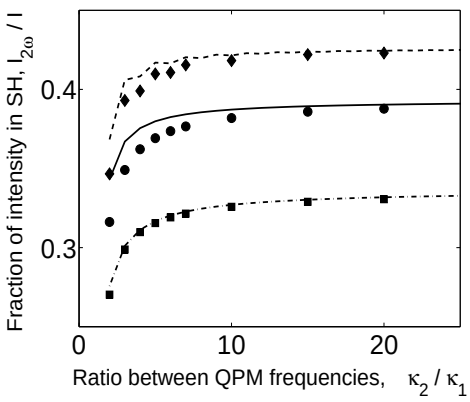

Fig. 6. Fraction of peak-intensity in SH at the first order resonances from Fig. 5. $\kappa_2 = 13$ and $\kappa_1 = p * 13$ (p is an integer). The input power is kept constant at $P = 15$ and $\epsilon = 0$. The lines represent theoretically predicted values whereas ♦, • and ■ are numerically measured values. Dashed line and ♦: Maximum value. Solid line and •: Average value. Dashed dotted line and ■: Minimum value. Notice that the lines actually represent the discrete integer values. They are drawn as lines just to help the eye.

initial transient has died out. Then we sample the minimum, maximum, and averaged peak intensities and compare those with the theoretically predicted values.

It is worth recalling that for every soliton solution of the reduced system (16-17) we have a whole family of solutions of the form (4-5). In Fig. 7 we have shown how one specific solution for $\tilde{\gamma} \approx 0.050$ leads to different initial conditions for two different physical setups. The two setups here chosen corresponds to the point ★ indicated on both Fig. 4 and Fig. 5. We also show the evolution of these initial conditions in Fig. 7, i.e. the evolution of the peak intensities.

For the induced averaged nonlinearities addressed in this paper to be of potential practical importance, they have to impact the observable soliton properties, including their excitation conditions. To show that this seems to be the case, in Fig. 8 we show the behavior found for the soliton content(38), SC, as a function of the residual phase mismatch in a two-period structure with QPM frequencies $(\kappa_1, \kappa_2) = (195, 13)$. We also include the outcome of the numerical experiments performed for a structure with the non-integer values $(\kappa_1, \kappa_2) = (194.7, 13.3)$, to show that the effect predicted is not restricted to a particularly suitable choice of these parameters. We launch a FF signal, with a sech-shape, and no SH seeding and calculate how much of the initial power, P_{in}, is bound in the soliton which eventually forms. We propagate until a steady state has emerged and then we collect the energy flow in a window wide enough to enclose substantially all the soliton. Typical values are propagation until $z = 10^3$ and collection of energy flow in a window of $x = \pm 10$, but these values were adapted whenever needed in order to capture always all the soliton energy. Simulations where carried out in the actual two-period QPM structure. The bandwidth of the SC for sech inputs can be estimated by using the Zakharov-Shabat scattering equations associated with the (1+1)-dimensional nonlinear Schrödinger equation, NLSE. With cubic terms, i.e. for

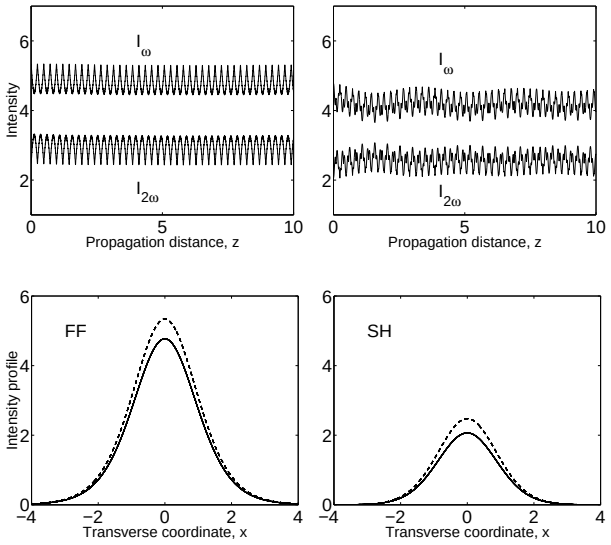

Fig. 7. Evolution of solitons in the real two-period system (1-2). Top figures show peak intensities. Bottom figures compare intensity profiles for the FF's (left) and SH's (right). Top left figure and dashed curves in bottom figures are for $(\kappa_1, \kappa_2) = (195, 13)$. Top right figure and solid curves in bottom figures are for $(\kappa_1, \kappa_2) = (32.9, 13)$). The two initial conditions stem from the same soliton of system (16-17) with $\tilde{\gamma} \approx 0.050$, $\epsilon = 0$, and $\lambda = 0.4$.

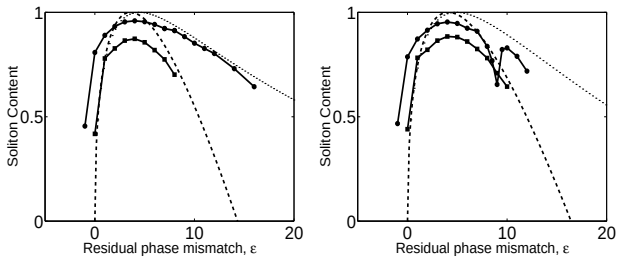

Fig. 8. Soliton content for sech input FF as a function of the residual phase mismatch $\epsilon = \beta - \kappa_1 - \kappa_2$ $(m = n = 1)$. Input power is $P_{in} = 50$. Left plot is for $(\kappa_1, \kappa_2) = (195, 13)$ $(\eta \simeq -0.38, \tilde{\gamma} \simeq 0.050)$ and right plot for $(\kappa_1, \kappa_2) = (194.7, 13.3)$ $(\eta \simeq -4/\pi^2, \tilde{\gamma} \simeq 0.038)$. •': SC for two-period QPM. '■': SC for purely quadratic model. The discrete points are the outcome of numerical experiments; the full lines in between are only to help the eye. The dashed and dotted lines are estimates from the limiting NLSE for a pure quadratic model and for a model with cubic terms, respectively.

system (8-9), one gets the estimate

$$\mathrm{SC} \simeq \frac{2\sqrt{\frac{\eta^2\epsilon}{\eta^2+\gamma\epsilon}}}{\eta^2 P_{in}} \left(\sqrt{2\eta^2 P_{in}} - \sqrt{\frac{\eta^2\epsilon}{\eta^2+\gamma\epsilon}} \right). \tag{21}$$

In the plot we also include the actual value of SC that is numerically found in the corresponding homogeneous pure quadratic case. Compared to the pure quadratic model, the bandwidth for the two-period structure is found to get wider. This effect can be understood by comparing the approximate theoretical expressions for the two cases given by (21). There is also an expected significant

increase in the efficiency owing to the fact that in systems with induced cubic terms the exited solitons are closer to the initial sech-shape than in purely quadratic systems. To explain the "dip" in the SC in the case of $(\kappa_1, \kappa_2) = (194.7, 13.3)$ again one must turn to the SHG spectrum. We find that the $(m = -1, n = 31)$-peak is located exactly at $\epsilon = 9.6$, which is where the bottom of the "dip" seems to be. Thus we conclude that the efficiency of soliton excitation is diminished because of resonances between the $(m = n = 1)$- and the $(m = -1, n = 31)$-peak.

In Fig. 9 we plot the soliton content for the $(\kappa_1, \kappa_2) = (195, 13)$ case, but now we scan mismatches not only around the $(m = n = 1)$-peak but also around the $(m = 1, n = -1)$-peak. In the absence of resonances and average cubic nonlinearities, i.e. $\eta = \pm 4/\pi^2$, no differences are found in the behavior of soliton excitation at each peak. However, such is not the case when the soliton generation efficiencies can interfere with each other, as shown in Fig. 9. For example, in the particular case shown, one observes that soliton generation around the $(m = 1, n = -1)$-peak takes place within a narrower band of mismatches and is less efficient than around the $(m = 1, n = 1)$-peak. This is because the average nonlinearities (14-15) are nonlinear functions of m and n and hence they change their relative strengths at the two peaks. A different behavior than that displayed in Fig. 9 might be obtained with different values of the two-grating periods and input light conditions, as shown in Fig. 10. When resonances are involved we note that at the $(m = 1, n = -1)$-peak the induced part of the average second order nonlinearity is stronger than the no-resonance value $4/\pi^2$ whereas it is weaker at the $(m = 1, n = 1)$-peak. Notice also that the soliton content vanishes in the intermediate region between the $(m = 1, n = \pm 1)$-peaks. This is because in the intermediate region between both peaks, e.g., at the mismatch that would be exactly compensated with a single-period QPM structure, the interference between the two peaks acts as a periodic amplitude modulation of the effective nonlinear coefficient, with a period comparable with the characteristic soliton length. Such modulation constitutes a very strong perturbation that prevents soliton formation.

We remark that one finds soliton generation around other peaks than the $(m = 1, n = \pm 1)$-peak. For example, in the $(\kappa_1, \kappa_2) = (195, 13)$ case we observe a band (not shown in the plot) around $\epsilon = 39$ corresponding to the $(m = 1, n = 3)$-peak. However, soliton formation in this band is much less efficient than in the $(m = 1, n = \pm 1)$-band and therefore we did not include it the plot. Similarly, other bands with higher QPM order also exist but one has to launch correspondingly high powers to excite solitons.

In conclusion, we derived an averaged model for the soliton propagation in two-period QPM systems of the form (8-9), and we showed that the model gives an accurate description of stationary soliton propagation under a variety of input light and material conditions. We have shown that one can use one grating period of the QPM structure to reduce the intrinsic phase mismatch and the other grating period to induce averaged cubic nonlinearities. We found the induced averaged cubic nonlinearities to be strongest when one QPM frequency is a multiple of the other, but we showed that those are

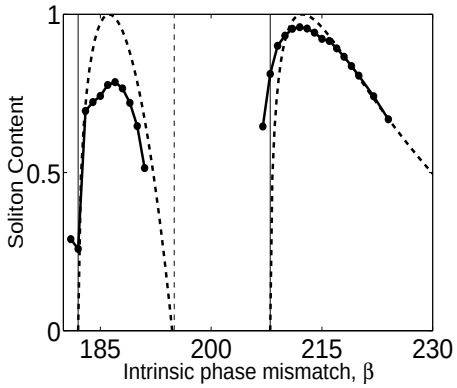

Fig. 9. Soliton content for sech input FF as a function of intrinsic phase mismatch β with $(\kappa_1, \kappa_2) = (195, 13)$. Input power is $P_{in} = 50$. The discrete points are the outcome of numerical experiments; the full lines in between are only to help the eye. The dashed curves are estimates from the limiting NLSE. The vertical lines located at $\beta = 182$ and $\beta = 208$ indicate the $m = 1, n = -1$ and $m = n = 1$ peaks, respectively. The dashed vertical line at $\beta = 195$ indicates the location of the peak in the absence of a second period (see Fig. 2).

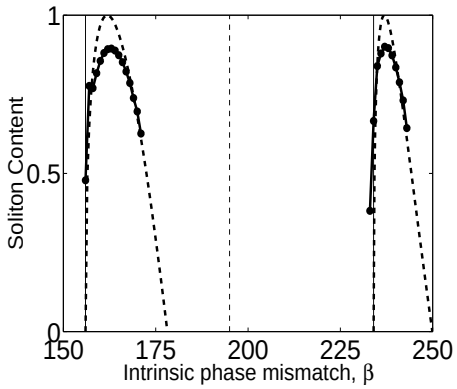

Fig. 10. Same as in Fig. 9, but here $(\kappa_1, \kappa_2) = (195, 39)$

.

strictly discrete resonances that cannot occur when experimentally feasible grating periods are taking into account. However, our investigations predict that also the no-resonance averaged contributions can be important. In particular, we found that the QPM engineered averaged cubic nonlinearities, induced in feasible two-period samples, enhances the peak-efficiency and residual mismatch-bandwidth of the soliton excitation process with non-soliton single frequency pump light.

Acknowledgements
This work was supported by the European Union through the Improving Human Potential program (contract HPRI-CT-1999-00071). Silvia Carrasco and Lluis Torner acknowledge support from the Generalitat de Catalunya, and by the Spanish government under TIC2000-1010. Ole Bang acknowledges support from the Danish Technical Research Council under Talent Grant No. 26-00-0355. Numerical work was carried out at CESCA-CEPBA-CIRI.

* Permanent address: Department of Informatics and Mathematical Modelling,

Technical University of Denmark, DK-2800 Lyngby, Denmark.

References

[1] R. L. Byer, Quasi-phasematched nonlinear interactions and devices, J. Nonlinear Opt. Phys. 6 (4) (1997) 549–592.

[2] M. M. Fejer, in *Beam shaping and control with nonlinear optics*, F. Kajzar and R. Reinisch, eds. (Plenum Press, New York, 1998), pp. 375-406.

[3] M. A. Arbore, M. M. Fejer, M. E. Fermann, A. Hariharan, A. Galvanauskas, D. Harter, Frequency doubling of femtosecond erbium-fiber soliton lasers in periodically poled lithium niobate, Opt. Lett. 22 (1) (1997) 13–15.

[4] M. A. Arbore, A. Galvanauskas, D. Harter, M. H. Chou, M. M. Fejer, Engineerable compression of ultrashort pulses by use of second-harmonic generation in chirped-period-poled lithium niobate, Opt. Lett. 22 (17) (1997) 1341–1343.

[5] P. Loza-Alvarez, D. T. Reid, P. Faller, M. Ebrahimzadeh, W. Sibbett, H. Karlsson, F. Laurell, Simultaneous femtosecond-pulse compression and second-harmonic generation in aperiodically poled $KTiOPO_4$, Opt. Lett. 24 (15) (1999) 1071–1073.

[6] G. Imeshev, M. A. Arbore, M. M. Fejer, Galvanauskas, M. Fermann, D. Harter, Ultrashort-pulse second-harmonic generation with longitudinally nonuniform quasi-phase-matching gratings: pulse compression and shaping, J. Opt. Soc. Am. B 17 (2) (2000) 304–318.

[7] G. Imeshev, M. Proctor, M. M. Fejer, Lateral patterning of nonlinear frequency conversion with transversely varying quasi-phase-matching gratings, Opt. Lett. 23 (9) (1998) 673–675.

[8] P. E. Powers, T. J. Kulp, S. E. Bisson, Continuous tuning of a continuous-wave periodically poled lithium niobate optical parametric oscillator by use of a fan-out grating design, Opt. Lett. 23 (3) (1998) 159–162.

[9] K. Mizuuchi, K. Yamamoto, M. Kato, H. Sato, Broadening of the phase-matching bandwidth in quasi-phase-matched second harmonic generation, IEEE J. Quantum Electron. 30 (7) (1994) 1596–1604.

[10] S.-N. Zhu, Y.-Y. Zhu, N.-B. Ming, Quasi-phase-matched third-harmonic generation in a quasi-periodic optical superlattice, Science 278 (1997) 843–846.

[11] K. Fradkin-Kashi, A. Arie, Multiple-wavelength quasi-phase-matched nonlinear interactions, IEEE J. Quantum Electron. 35 (11) (1999) 1649–1656.

[12] M. H. Chou, K. R. Parameswaran, M. M. Fejer, I. Brener, Multiple-channel wavelength conversion by use of engineered quasi-phase-matching structures in $LiNbO_3$ waveguides, Opt. Lett. 24 (16) (1999) 1157–1159.

[13] H. Liu, Y. Y. Zhu, S. N. Zhu, C. Zhang, N. B. Ming, Aperiodic optical superlattices engineered for optical frequency conversion, Appl. Phys. Lett. 79 (6) (2001) 728–730.

[14] J. Capmany, Simultaneous generation of red, green, and blue continuous-

wave laser radiation in Nd^{3+}-doped aperiodically poled lithium niobate, Appl. Phys. Lett. 78 (2) (2001) 144–146.
[15] M. Cha, Cascaded phase shift and intensity modulation in aperiodic quasi-phase-matched gratings, Opt. Lett. 23 (4) (1998) 250–252.
[16] K. Gallo, G. Assanto, K. R. Parameswaran, M. M. Fejer, All-optical diode in a periodically poled lithium niobate waveguide, Appl. Phys. Lett. 79 (3) (2001) 314–316.
[17] L. Torner, C. B. Clausen, O. Bang, P. L. Christiansen, Y. S. Kivshar, M. M. Fejer, Soliton control by QPM engineering, Optics & Photonics News 10 (12) (1999) 44.
[18] L. Torner, C. B. Clausen, M. M. Fejer, Adiabatic shaping of quadratic solitons, Opt. Lett. 23 (12) (1998) 903–905.
[19] C. B. Clausen, O. Bang, Y. S. Kivshar, Spatial solitons and induced Kerr effects in QPM media, Phys. Rev. Lett. 78 (1997) 4749–4752.
[20] C. B. Clausen, L. Torner, Spatial switching of quadratic solitons in engineered quasi-phase-matched structures, Opt. Lett. 24 (1) (1999) 7–9.
[21] C. B. Clausen, O. Bang, Y. S. Kivshar, P. L. Christiansen, Quasi-periodic envelope solitons, Phys. Rev. Lett. 83 (23) (1999) 4740–4743.
[22] S. Carrasco, J. P. Torres, L. Torner, R. Schiek, Engineerable generation of quadratic solitons in synthetic phase matching, Opt. Lett. 25 (17) (2000) 1273–1275.
[23] O. Bang, C. B. Clausen, P. L. Christiansen, L. Torner, Engineering competing nonlinearities, Opt. Lett. 24 (1999) 1413–1415.
[24] J. F. Corney, O. Bang, Solitons in quadratic nonlinear photonic crystals, Phys. Rev. E 64 (4) (2001) 047601.
[25] A. Kobyakov, F. Lederer, O. Bang, Y. S. Kivshar, Nonlinear phase shift and all-optical switching in quasi-phase-matched quadratic media, Opt. Lett. 23 (7) (1998) 506–508.
[26] O. Bang, T. W. Graversen, J. F. Corney, Accurate switching intensities and length scales in quasi-phase-matched materials, Opt. Lett. 26 (13) (2001) 1007–1009.
[27] J. F. Corney, O. Bang, Modulational instability in periodic quadratic nonlinear materials, Phys. Rev. Lett. 87 (13) (2001) 133901.
[28] A. V. Buryak, Y. S. Kivshar, S. Trillo, Optical soliton supported by competing nonlinearities, Opt. Lett. 20 (19) (1995) 1961–1963.
[29] O. Bang, Dynamical equations for wave packets in materials with both quadratic and cubic responses, J. Opt. Soc. Am. B 14 (1997) 51–61.
[30] L. Bergé, O. Bang, J. J. Rasmussen, V. K. Mezentsev, Self-focusing and solitonlike structures in materials with competing quadratic and cubic nonlinearities, Phys. Rev. E 55 (3) (1997) 3555–3570.
[31] O. Bang, L. Bergé, J. J. Rasmussen, Wave collapse in bulk media with quadratic and cubic responses, Opt. Commun. 146 (1998) 231–235.
[32] O. Bang, Y. S. Kivshar, A. V. Buryak, A. D. Rossi, S. Trillo, Two-dimensional solitary waves in media with quadratic and cubic nonlinearity, Phys. Rev. E 58 (4) (1998) 5057–5069.
[33] A. S. Helmy, D. C. Hutchings, T. C. Kleckner, J. H. Marsh, A. C. Bryce, J. M. Arnold, C. R. Stanley, J. S. Aitchison, C. T. A. Brown, K. Mout-

zouris, M. Ebrahimzadeh, Quasi phase matching in GaAs-AlAs superlattice waveguides through bandgap tuning by use of quantum-well intermixing, Opt. Lett. 25 (18) (2000) 1370–1372.

[34] Y. Shuto, T. Watanabe, S. Tomaru, I. Yokohama, M. Hikita, M. Amano, Quasi-phase-matched second-harmonic generation in diazo-dye-substituted polymer waveguides, IEEE J. Quantum Electron. 33 (3) (1997) 349–357.

[35] L. Torner, J. P. Torres, O. Bang, Robustness of quadratic solitons with periodic gain, Opt. Commun. 185 (2000) 479–485.

[36] C. R. Menyuk, R. Schiek, L. Torner, Solitary waves due to $\chi^{(2)} : \chi^{(2)}$ cascading, J. Opt. Soc. Am. B 11 (12) (1994) 2434–2443.

[37] Y. S. Kivshar, N. Grønbech-Jensen, R. D. Parmentier, Kinks in the presence of rapidly varying perturbations, Phys. Rev. E 49 (5) (1994) 4542–4551.

[38] L. Torner, J. P. Torres, D. Artigas, D. Mihalache, D. Mazilu, Soliton content with quadratic nonlinearities, Opt. Commun. 164 (1999) 153–159.